Estimating Annual Global Upper Ocean Heat Content Anomalies Despite Irregular In Situ Ocean Sampling[*,**]

JOHN M. LYMAN[1,2] AND GREGORY C. JOHNSON[2]

[1] *Joint Institute for Marine and Atmospheric Research, University of Hawaii*

[2] *NOAA/Pacific Marine Environmental Laboratory, Seattle, Washington*

Submitted to *Journal of Climate*

26 September 2007

Corresponding author address:

John M. Lyman, Pacific Marine Environmental Laboratory, NOAA/R/PMEL, 7600 Sand Point Way, Seattle,WA 98115 (email:John.Lyman@noaa.gov)

* Pacific Marine Environmental Laboratory Contribution Number 3123

** Joint Institute for Marine and Atmospheric Research contribution Number 07–367.

ABSTRACT

The effects of irregular in situ ocean sampling on estimates of annual globally integrated upper Ocean Heat Content Anomalies (OHCA) are investigated for sampling patterns from 1955 to 2006. An analytical method is presented for computing the effective area covered by an objective map for any given in situ sampling distribution. To evaluate the method, appropriately scaled sea surface height (SSH) anomaly maps from Aviso are used as a proxy for OHCA from 1993 to 2006. Use of these proxy data demonstrates that the simple area integral of such an objective map for sparse data sets does not agree as well with the actual integral as a representative one, defined as the simple integral muliplied by the ratio of the total area over the effective area for that map. From 1955 to 1966, in situ ocean sampling is inadequate to estimate accurately annual global integrals of upper OHCA. During this period, simple integrals for the sampling pattern of any given year underestimate the 13-year trend in proxy OHCA from 1993 to 2006 by around 70%, and confidence limits for representative integrals are often very large. From 1967 to 2003 there appear to be sufficient data to estimate annual global integrals. For this time period the simple integrals for any given year's sampling pattern still underestimate the 13-year trend by around 30%, but the representative integrals match the trend well with small confidence limits. For 2004 through 2006 in situ sampling, with near-global in situ Argo data coverage, the 13-year trend is equally well represented by simple or representative integrals.

1. Introduction

Most of the Earth's warming signal arising from anthropogenic climate change is thought to reside in the upper ocean (Hansen et al. 2005; Levitus et al. 2005). To understand past and present global warming trends, and so to provide data for improvement of predictions of future changes, it is necessary to refine estimates of global upper Ocean Heat Content Anomalies (OHCA) and their uncertainties. Here the effect of the irregular sampling of the world's ocean over the last half-century on annual global OHCA estimates is quantified, and a method that may improve them is proposed.

There are several ways to compute the global integral of mapped in situ data (Wunsch et al. 2007; Gille 2007). Two of them are compared here. One of these is a straightforward area integral of objectively mapped data. Because objective maps generally relax back towards the mean in data-sparse regions, this method generally assumes zero anomalies in regions that are not sampled. It will be referred to as the integral of the map throughout this paper. The second method is effectively an area integral only over regions with good data coverage divided by the fraction of the ocean used in the integral. This method assumes that the spatial mean of the anomalies in the un-sampled regions is the same as the mean for the sampled regions. It will be referred to as the representative integral throughout the paper.

Irregular historical in situ sampling of the oceans in both space and time complicates model data intercomparisons. For instance, the variability in the global integral of upper OHCA depends on how data-poor regions are treated when

integrating. It turns out that simple global OHCA integrals of objective maps have different variability than representative integrals (Gregory et al. 2004; AchutaRao et al. 2006; Gille 2007) making it difficult to validate the warming signal in a given model by comparing globally integrated model OCHA products to simple integrals of data-based OHCA maps. Furthermore, local regional trends in OCHA are large and variable, with some regions cooling for a time while other regions warm (e.g., Harrison and Carson 2007). This variability, combined with sparse data coverage, has led some to conclude that historical data may not be sufficient to discern a global warming trend (Harrison and Carson, 2007).

One method used to improve comparisons of models with existing data is to sample model output at the same locations and times where the actual ocean is sufficiently well sampled (e.g., Gregory et al. 2004; AchutaRao et al. 2006; Pierce et al. 2006). In these comparisons subjective criteria have been used to select areas where the number of observations is deemed sufficient to make a comparison. Representative integrals generated from observational data and identically sampled model output can significantly improve agreement in OCHA comparisons. These comparisons suggest that these models are doing a good job of simulating global ocean heat content increases that are primarily due to anthropogenic climate change.

This agreement withstanding, in situ ocean observation-based estimates of the globally integrated OHCA timeseries are a useful model benchmark and an important diagnostic for changes in the Earth's climate system (Hansen et al. 2005; Levitus et al. 2005). Recently observational estimates of the global integral of OHCA tend to be calculated as integrals of objective maps (Willis et al. 2004; Levitus et al. 2005; Ishii et

al. 2006). While the complexity and sophistication of these objective analyses varies, they nearly all have anomalies that relax toward zero in areas of sparse data coverage. The integrals of these maps are affected by this tendency. Here a method for computing the area in an objective map is derived (Appendix A) to allow estimation of representative integrals from objectively mapped data.

The simple integrals of the maps and representative integrals are compared side by side. To quantify the effects of irregular sampling on these integrals delayed mode Aviso satellite sea surface height (SSH) anomalies are scaled appropriately to produce a synthetic data-based proxy for the global upper OHCA record from 1993 through 2006. Satellite SSH fields are not truly global, have possibly undefined errors, and along with heat content, include signals from freshwater variations and deep variability (Willis et al. 2004; Wunsch et al. 2007). These potential complications notwithstanding, the SSH maps constitute a useful, continuous, high-resolution, and nearly global observational record over the ice-free oceans that have been shown to be correlated with in situ upper ocean OHCA observations (White and Tai 1995; Gilson et al. 1998; Willis et al. 2004). For the purpose of this analysis, the synthetic estimate of OHCA from SSH is considered the true global estimate of OHCA. The synthetic OHCA record from 1993 through 2006 is subsampled at the locations and time of the year that in situ data were collected for all years between 1955 to 2006 to see how yearly sampling patterns affect both the linear trend in globally integrated OCHA from 1993 to 2006 and sampling errors on the global integrals during those years.

Here the focus is on how historical sampling of world oceans affects global annual OHCA values and their errors along with developing and evaluating an

appropriate scheme for constructing representative integrals of OCHA maps from in situ data. Unknown, potentially large, and difficult to quantify instrument biases that may affect the SSH fields (Wunsch et al. 2007) are ignored. Possible errors in the covariance function and the climatology that could impact estimates of upper OHCA based on in situ data (AchutaRao et al. 2007; Wunsch et al. 2007) are also ignored.

The data used to define the in situ sampling distribution, the satellite SSH anomaly fields used as a proxy for upper OCHA, and the objective mapping techniques are discussed in section 2. The spatial and temporal structure of the data distribution are analyzed in section 3. The effects of irregular sampling are investigated on 13-year trends in section 4 and 3- to 13-year trends in section 5. An estimate of the sampling error on the global integral of OHCA is computed in section 6. The results are discussed and summarized in section 7.

2. Data and mapping

In situ ocean temperature measurements are a mixture of data from reversing thermometers used during hydrographic stations, Mechanical BathyThermograph (MBT) profiles, eXpendable Bathythermograph (XBT) profiles, ship board conductivity-temperature-depth (CTD) profiles, moored buoy thermistor records (many from the Tropical Atmosphere Ocean array), and autonomous profiling CTD float data (primarily from Argo). The data used here were obtained from the World Ocean Database 2005 (Boyer et al. 2006), the Global Temperature & Salinity Profile Project (GTSPP), and the Argo Global Data Assembly Centers. Because of known but as yet not completely resolved biases among data from different instrument types (AchutaRao

et al. 2007; Gouretski and Koltermann 2007; Wijffels et al. 2007; Willis et al. 2007b), no attempt is made here to produce a heat content curve from in situ observations. Instead the effects of irregular sampling are analyzed using a synthetic estimate of OHCA from sea surface height (SSH).

Nonetheless, the in situ data were subject to some basic quality control (QC) procedures to identify valid in situ data locations in the historical record. In order to remove duplicates between the different databases, profiles within 15 minutes in time and 3.6 arc seconds in space were removed from the GTSPP. This process was repeated twice. Profiles with insufficient vertical resolution were also discarded. To have sufficient vertical resolution, the upper 400 m of the profiles had contain at least 6 data points flagged as good, a good measurement in the upper 30 m, a maximum good measurement depth exceeding 300 m, and depth spacing no more than twice that of the standard depths used in the World Ocean Database. Retained profiles were then subject to further QC in World Meteorological Organization (WMO) squares. Squares with small numbers of profiles were combined. Then, by visual inspection, profiles with obviously spurious data compared to the bulk of the data in each square were discarded. Finally, OHCA estimates within these squares that fell outside of four standard deviations were discarded.

Mapped satellite SSH anomaly estimates came from combined Aviso SSH. This product is an optimal merging of SSH from multiple platforms: Topex/Poseidon, Jason, ERS-1/2, and Envisat. The resulting product has 10-day temporal and approximately 150–200 km spatial resolution (Ducet et al. 2000). In this analysis SSH anomalies are used as a surrogate for upper ocean heat content anomalies by exploiting

the strong correlations between SSH anomalies and available in situ estimates of OHCA (White and Tai 1995; Gilson et al. 1998; Willis et al. 2004; Lyman et al. 2006). These correlation coefficients vary geographically. However, here a global average correlation coefficient of 51 zeta-joules cm^{-1} is used (Lyman et al. 2006).

Objective mapping (e.g., Wunsch 1996) covariance functions, correlation length scales, and signal-to-noise ratios used here follow those adopted by Willis et al. (2004) and used again in Lyman et al. (2006). These techniques, functions, and values apply to both the objective maps generated from subsampled Aviso SSH fields and to the fraction of area coverages computed for these maps (Appendix A). Following Willis et al. (2004), the record-length mean is removed from each location from the SSH fields. Then, the annual cycle, in this cased based on quarterly means of the 1993–2006 anomalies of the Aviso SSH record, is removed. The resulting fields are then subsampled at the location and time of the year for a given year's in situ data sampling and grouped into 1-year bins centered on the middle of each year. These grouped data are then spatially mapped. The mapping is a simple objective map containing both a small scale (~ 100 km) and a large scale (~1000 km) in its covariance function (Willis et al. 2004). The correlation function also includes an error along the diagonal, to account for variability at time scales less than a year.

3. Data distribution

In situ upper ocean sampling has varied substantially both spatially and temporally over the last half-century. Between 1955 and 1966, the percentage of the ice-free upper ocean sampled increased from near 20 to 40% (Fig. 1). With widespread

XBT use starting in 1967, the fraction of the ocean represented in that year's annual map rose to 48%. This fraction continued to rise to around 75% during the 1980's and 1990's as programs such as the World Ocean Circulation Experiment (WOCE) were implemented. WOCE spun down in the late 1990's, and the sampling area decreased to 63% by 2000. Some of this decrease may be eliminated for the last decade once data has made its way from originators to the World Ocean Database, as there can be a multi-year lag for this process. In addition, efforts to gather historical data by NOAA's National Ocean Data Center have and should continue to help to increase data coverage in past years. The percentage of area sampled increases again after 2000 as more and more Argo autonomous profiling CTD floats began reporting data in real time. For every suceeding year since 2004, as Argo has been approaching its target of global sampling with 3000 active floats, the area sampled has been a record, with 89% coverage reached in 2006.

The method for computing area (see Appendix A) takes into account the covariance functions, correlation length scales, and error energies used in the objective mapping described in Section 2 to compute the area of the ocean sampled. This method contrasts with the frequent use of arbitrary criteria on number of observations in an averaging bin to select bins with sufficient measurements for use in computation of a representative integral or other quanitity. The data-based estimate of error energy added to the diagonal of the correlation function results in a low area coverage in regions with few observations.

The spatial distribution of observations evolves with changing methods of data collection. In the pre-XBT era, here analyzed starting in 1955 and ending in 1966, the

upper ocean was sparsely sampled. Most of the observations were concentrated near coastlines in the northern hemisphere (Fig. 2). As XBTs came into use, the spatial coverage dramatically increased from 1967 through 2003 (Fig. 3). For this period most of the northern hemisphere is well sampled with contrasting sparse coverage in the southern hemisphere, where shipping lanes are more widely spaced. From 2004 through 2006, Argo profiling CTD float data provide a fairly even spatial distribution of data for in situ OHCA estimates (Fig. 4).

Aviso SSH maps are available from 1993 through 2006. During this period in situ sampling of OHCA changed from primarily XBT data along shipping route to more even global coverage by the autonomous profiling CTD floats of Argo. This change is evident in the standard deviation of the effective sampling areas for annual objective maps of in situ OCHA data during this time period (Fig. 5). Large sampling variations are evident south of about 40°S in the Pacific Ocean, and even further north in parts of the South Atlantic and Indian Oceans. The irregular and poor sampling in the Southern Ocean prior to Argo contributes to uncertainty of global OHCA integrals (AchutaRao et al. 2007; Gille 2007). For example, sparse and seasonally biased sampling in the Southern Ocean could corrupt the estimates of means and seasonal cycles, and thus annual OHCA estimates. While these are real and important problems, they are not investigated here nor do they affect the results presented here, as the Aviso SSH records used here as a proxy for OHCA are well resolved.

4. 13-year warming trends

The fully resolved synthetic SSH estimate of the upper OHCA curve has a warming trend of 0.9 ± 0.1 W m^{-2} from 1993 through 2006 (Fig. 6, grey line), as estimated by a linear fit. Here and throughout the paper, OHCA trends are estimated by linear fits and are normalized to the area of the earth (Levitus et al. 2005; Lyman et al. 2006). Trend errors are expressed as 95% confidence intervals of the slopes of those linear fits. As mentioned in section 2, the synthetic estimate contains signals besides just upper OHCA (most obviously, changes in ocean mass) and is likely an overestimate of the true warming of the upper ocean (Willis et al. 2004).

To examine the effects of irregular sampling on the 13-year warming trend, the synthetic upper OHCA was subsampled at the in situ data locations from 1993 to 2006. The resulting data were mapped and then spatially integrated. When spatially integrating the subsampled global OHCA maps it is necessary to define the method of computing a global integral (Appendix A). Two of the simplest choices are (1) the integral of the maps, where OHCA values are assumed to tend toward zero in locations and times where there are few measurements; and (2) a representative integral, where the value of OHCA in regions where it is not measured is assumed to be the same as the global mean of that value in the regions where it is measured (Appendix A).

Both of the methods are able to produce a trend within the confidence interval on the true synthetic trend (Fig. 6). Integrals of the maps underestimate the trend at 0.8 ± 0.1 W m^{-2} while representative integrals overestimate the trend at 1.0 ± 0.1 W m^{-2}. Neither trend estimate is significantly different from the trend for the fully resolved data set, but individually they barely agree with each other. While this assessment of

how the in situ sampling from 1993 through 2006 reproduces the warming trend over that period is useful, it says little of how the different sampling eras and integration assumptions affect the estimates of the trend.

By subsampling every year of the 13-year synthetic upper OHCA like the data distribution for a given year, it is possible to construct a 13-year time series of annual upper OHCA estimates for that single year's sampling pattern. This subsampling strategy differs from the one just presented in that it yields an annual upper OHCA time-series from 1993 through 2006 for each year's data distribution. The results can be used to estimate sampling errors for any given year and assess the two different methods for global integration of OHCA. Because this strategy depends only on knowing the sampling pattern for the year under study, it can be applied to assess errors associated with historical sampling for years before Aviso SSH was available. The estimates of the trend for historical sampling before 1993 are only applicable to the real trend in as much as the 1993 to 2006 period represents the time period in which the data were taken.

Integrals of the maps for sparse historical sampling patterns generally produce underestimates of the actual 1993–2006 warming trend. For instance, the very sparse 1955 sampling pattern produces a very low, 0.1 ± 0.1 W m^{-2} (Fig. 7, upper panel), estimate of the 13-year warming trend from the integrals of the maps. This estimate is only a small fraction of the true warming trend of 0.9 ± 0.1 W/m^{-2}. Even the much better sampling pattern for 1995 results in integrals of the maps for the 1993–2006 period that estimate a warming trend, 0.7 ± 0.1 W m^{-2}, (Fig. 7, lower panel) that is significantly less than the true trend.

In situ ocean sampling patterns for every year (but the last few years) of the last half century result in significant underestimates of the 1993–2006 warming trend using simple integrals of the maps (Fig. 8). In the pre-XBT area of sampling, 1955–1966, the warming estimates range from 10–50% of the true trend. The fraction of the trend estimated from integrating the maps increases slowly to about 75% of the true trend from 1967 – 2003. It is not until the Argo array approaches sparse global coverage in 2004 that the warming trend estimated from the integrals of the maps for that year's sampling pattern is within the 95% confidence interval of the true synthetic warming rate. The 95% confidence interval for the linear trend estimate from the simple integrals of the maps stays near ±0.1 W m^{-2} for all of the 53 years of data coverage (Fig. 8, lower panel).

Estimates of the global warming trend in annual upper OHCA from representative integrals are always within the confidence interval on the true trend (Fig. 8, upper panel). For pre-1967 sampling patterns, the trend estimates from representative integrals oscillate noticeably about the true estimate. For post-1967 sampling patterns the trend estimates are remarkably close to the true trend. While representative integrals produce an estimate closer to the true trend, the process of dividing by fraction of area sampled (Appendix A) can significantly increase the 95% confidence intervals for that estimate (Fig. 8, lower panel). This increase is largest when the data coverage is sparsest. For instance, the 95% confidence intervals for the trend estimate from representative integrals for the 1955 sampling pattern are 7 times larger than the confidence intervals for the trend from the fully resolved data set. As the data coverage increases, the confidence interval on the trend estimated from the

representative integrals decreases, reaching twice the true level in 1967 and finally approaching the true level by the 1990's.

5. Three- to 13-year trends

The method of computing the integral also affects how well the historical in situ sampling patterns reproduce linear warming trends over intervals between 3 and 13 years. As for the 13-year trend, the fidelity and confidence intervals for warming trends over these shorter intervals are examined by subsampling the synthetic upper OHCA.

A composite of estimated trends is used to examine how well different time scales are reproduced during different eras of sampling. This analysis is done by estimating the linear trend from different segments of the 13-year synthetic upper OHCA curve for each sampling pattern from 1955 to 2006. The shorter the trend, the more estimates of a particular sampling distribution. The results of these fits are summarized by era (Figs. 9–10).

For all time scales, before the widespread use of the Argo floats (1955 to 2003), representative integrals are able to reproduce the real trend within the confidence interval while integrals of the maps produce trends that are well below those of the true values (Fig. 9). In the pre-XBT era, 1955 to 1966, integrals of the maps underestimate the true trends by 0.6 to 0.7 W m^{-2} for all time scales (Fig. 9, upper panel). Representative integrals during that same era only underestimate the true trend by <0.1 W m^{-2}, well within 95% confidence intervals for the true values. Unlike those for the trends produced from integrals of the maps, the confidence level on the trends from

representative integrals are strongly dependent on time scale. At shorter time scales, 95% confidence limits are near 0.8 W m^{-2}, close to the true 13-year warming trend of 0.9 W m^{-2}. At longer time scales the 95% confidence intervals for trends estimated from representative integrals approach 0.3 W m^{-2}.

As the sampling increases during the XBT era (1967 to 2003), the mean difference from the true warming trend also decreases (Fig. 9, lower panel). Simple integrals of the maps produce trends that are an underestimate of about 0.3 W m^{-2} at all times cales. These trends lie near the outside edge of the 95% confidence interval. Alternatively, the linear trends produced from the representative integrals during the XBT era match the true trend within ±0.01 W m^{-2}, indicating that trends estimated from the representative integrals are effectively the same as the true trends. The means of the trends produced from the representative integrals all lie well within the 95% confidence intervals, which, as in the pre-XBT era, start out large (0.3 W m^{-2}) for shorter time scales but decrease to about 0.1 W m^{-2} for longer time scales.

When Argo provided near-global coverage (2004–2006), trends estimated from the representative integrals overestimated the true trends by about 0.05 W m^{-2} for all time scales studied (Fig. 10). In contrast, trends estimated from the integrals of the maps are underestimates by about 0.1 W m^{-2} for all time scales. For both methods of computing the integrals, the trends estimated by mapping subsampled data agree with the "true" trends within 95% confidence intervals.

6. Sampling error

Sampling error is estimated from the standard deviation of the difference between true values of annual globally integrated upper OHCA and estimates based on simple integrals of the maps or representative integrals (Lyman et al. 2006). Because the data sets have been updated, a slightly more stringent QC has been employed, and 2 more years of delayed mode Aviso data have been added since that study, the sampling errors presented here for the integrals of the maps are slightly larger than those shown in Lyman et al. (2006). Sampling errors computed from the representative integrals are less than those computed from the integrals of the maps for most of the record (Fig. 11). The larger errors from the integrals of maps are a reflection of the large underestimates of the trends (see section 3).

Over both the pre-XBT and XBT eras, the integrals of the maps produce sampling errors that are about twice those of the representative integrals. The exception is 1955, when the noise introduced by the use of representative integrals is larger than that introduced by the underestimated trend. From 2004 to 2006, as global coverage increases, the two estimates converge.

Sampling error decreases as the sampling area increases. Sampling error starts out high in 1955: 50 zeta joules for the integrals of the maps and 60 zeta joules for the representative integrals. As XBTs come into wide use after 1967 sampling errors level out near 20 zeta joules for integrals of the maps and 10 zeta joules for representative integrals. Finally, with the Argo array approaching its target of near-global sampling with 3000 profiling CTD floats, the different estimates of the sampling error overlap near 5 zeta joules in 2005 and 2006.

7. Discussion and conclusions

Irregular sampling of the Earth's oceans from 1955 to 2006 impacts estimates of interannual to decadal trends of global integrals of upper OHCA. The impact depends on the method used to estimate the global integrals. Integrals of annual maps made from an OHCA proxy between 1993 and 2006 using sampling patterns from a given year are computed using two different methods. Warming trends in the global integral of upper OHCA on timescales between 3 to 13 years are significantly underestimated using simple integrals of the maps but are consistently estimated within 95% confidence limits using representative integrals. From 2004 through 2006, as Argo begins to approach providing global coverage, the estimates of trends using either method with those years' sampling patterns converge, and agree with the true estimates within 95% confidence intervals.

For the time scales investigated in this paper, there is not sufficient in situ data coverage before 1967 to estimate the global integral of upper OHCA, regardless of the method used to compute the spatial integral. For sampling patterns from this pre-XBT era, spatial integrals based on simple integrals of the maps grossly underestimate the true trend for 1993–2006 by 0.7 W m^{-2} or 70% (Fig. 8). On the other hand, representative integrals mask the true trend by increasing the noise. The consequence is an increase in the 95% confidence interval to 0.6 W m^{-2} for the 1955 sampling pattern, or 66% of the true slope (Fig. 8). Given pre-XBT sampling patterns, neither of these methods is adequate to estimate the true 13-year linear trend of 0.9 ± 0.1 W m^{-2}.

After the introduction of the XBT, but before Argo began providing global coverage (1967 to 2003), the sampling density increased and the errors on the trend decreased, so that the 95% confidence interval for the 13-year warming trend was about 0.1 W m^{-2} using either the integrals of the maps or the representative integrals. During this era, the integrals of the maps significantly underestimate the 13-year trend by 0.3 W m^{-2} or 30% (Fig. 8). Conversely, the representative integrals accurately reproduce the 13-year trend within the 95% confidence interval.

For the most recent sampling distribution (2004 to 2006), with Argo approaching the goal of near-global sampling, the annual global integral of OHCA is accurately estimated at all scales regardless of spatial integration method (Fig. 10). Interestingly the representative mean tends to slightly (but insignificantly) overestimate the trend during the Argo sampling era. This slight discrepancy could be due to either an overestimate of the error energy used in the objective maps or because under-sampled regions warmed at a slower rate than well-sampled regions.

Of the two methods for computing global integrals considered in this paper, representative integrals appears to produce more accurate estimates of the global integral of OHCA than simple integrals of the maps. This result is consistent with analyses showing that the Southern Ocean, the largest area where the representative integral fills in with a global warming trend, has indeed warmed in the last decade (Gille 2007). These results suggest that the representative integral is the preferable method for estimating historical OHCA global integrals at annual time scales. However, it is important to remember that these results are based on how well in situ sampling reproduces trends in Aviso SSH anomalies, which are here scaled for use as a

proxy for upper OHCA. It seems likely, for example, that the global integral of SSH includes a significant large-scale freshwater component in addition to thermosteric expansion (Wunsch et al. 2007). It is also conceivable that interannual variability in globally integrated OHCA may have been underestimated by the SSHA proxy. If this were so, the error in the slope from the representative integrals would be disproportionately underestimated compared to the slope computed from the integrals of the maps.

While it may not be certain that the representative integrals are preferable, it has been shown that the two integration methods can produce significantly different results, both of which should be used in examining historical trends in OHCA if for nothing more than to quantify the sensitivity of the estimates to different methods of computing global integrals.

Integrals of the map might agree more closely with representative integrals for sparse sampling patterns were the mapping correlation function to contain a global length scale. However, introducing a global scale into the inversion would be prohibitively time consuming, and does not have an obvious physical basis. The representative integrals here are computationally feasible, and make explicit the assumption that where data coverage is low, the mean anomaly is assumed in essence to be equal to the global mean where data coverage is adequate.

Sampling errors from 1967 to 2006 are adequate to estimate trends in OHCA (Fig. 11). Prior to 1967, both the integrals of the maps and the representative integrals produce large errors in globally integrated upper OCHA reaching 60 zeta joules in 1955 with the representative integral. The errors computed from the representative integrals

are likely a more realistic representation of the sampling error than those from the integrals of the maps, in that the errors computed from the representative integrals come from the scatter about the true value, whereas the errors from the integrals of the maps reflect an underestimation of the warming trend.

Applying these methods to sampling patterns for any year prior to 1993 indicates how well the historical sampling for that year would have performed in estimating the global integral and its trend over the 13-years of Aviso SSH were that sampling pattern repeated yearly. Trends in OHCA vary from decade to decade and location to location (Harrison and Carson 2007). These decadal changes make estimates of pre-1993 sampling errors likely to be only a rough approximation of the true sampling errors.

In terms of the sampling errors, in situ sampling patterns from 1967 to 2006 appear to be adequate to estimate trends in globally integrated upper ocean OHCA, especially if a representative integral is used for the pre-Argo years when coverage was not truly global. However, sampling errors are only one portion of the error budget. Biases in the mean climatology or instrument biases which are difficult to detect and quantify could be large (AchutaRao et al. 2007; Gouretski and Koltermann 2007; Willis et al. 2007a; Wunsch et al. 2007). Currently the structure of the globally integrated OHCA curve is uncertain, primarily due to an apparent temporal bias in the eXpendable BathyThermograph (XBT) data (Gouretski and Koltermann 2007) that is plausibly owing to temporal variations in XBT fall rates (Wijffels et al. 2007), along with a correctable error in about 7% of the Argo profiling floats (Willis et al. 2007a, b). It appears that rectification of these biases will act to reduce interannual variability in the

OHCA curve, but the best corrections may not yet be established. For these reasons, an in situ estimate of global integral of OHCA is not computed here.

Acknowledgments. Altimeter products used herein were produced by Ssalto/Duacs as part of the Environment and Climate EU Enact project (EVK2–CT2001–00117) and distributed by Aviso, with support from CNES. The bulk of the in situ data used herein was provided through the World Ocean Database 2005 and the Global Temperature-Salinity Profile Program (http://www.nodc.noaa.gov). Float data were collected and made freely available by Argo (a pilot program of the Global Ocean Observing System) and contributing national programs (http://www.argo.net/). Helpful comments were provided by Carl Wunsch, Bruce Cornuelle, and Josh Willis. The NOAA Climate Program Office and the NOAA Office of Oceanic and Atmospheric Research provided support for this research. The findings and conclusions in this article are those of the authors and do not necessarily represent the views of the National Oceanic and Atmospheric Administration.

APPENDIX A

Two global integrals

An ideal global integral can be defined as $\sum_{\substack{i=0,I \\ j=0,J}} true_{i,j} dA_{i,j} = I_t$, where I_t is the true integral, and $true_{i,j}$ the true value that represents the area $dA_{i,j}$ at a location i, j. The true field can be separated into a mean and anomaly, $true_{i,j} = true'_{i,j} + m_t$, where A is the area of the ocean and $true'_{i,j}$ are the spatial anomalies relative to a true spatial mean, m_t, such that $\sum_{\substack{i=0,I \\ j=0,J}} true'_{i,j}\, dA_{i,j} = 0$. Hence,

$$I_t = m_t A, \tag{A1}$$

where m_t is estimated from the a set of k observations, obs_k.

Given the spatial distribution of obs_k an objective mapping (e.g., Wunsch 1996) can be defined, $\langle obs_k \rangle_{i,j}$, where $\langle\ \rangle_{i,j}$ is an objective map to a location i, j. The spatial integral of the mapped observations is then,

$$I_o = \sum_{\substack{i=0,I \\ j=0,J}} \langle obs_k \rangle_{i,j} dA_{i,j}. \tag{A2}$$

a. Integral of the map

The simplest way to define a spatial integral is in terms of an area weighted integral of the mapped observations. Here the mapped observations are defined on the

map grid as, $\langle obs_k \rangle_{i,j} \equiv \langle obs_k' \rangle_{i,j} + m_{map}$, such that $\sum_{\substack{i=0,I \\ j=0,J}} \langle obs_k' \rangle_{i,j} dA_{i,j} \equiv 0$ and m_{map} is the mean of the map. When substituted into (A2) these equations yield

$$m_{map} = \frac{I_o}{A}. \tag{A3}$$

If m_t is estimated by m_{map} then by substituting (A3) into (A1) the true integral can be estimated by the integral of the map,

$$I_t \approx I_o \ . \tag{A4}$$

This method intrinsically assumes that the data distribution is adequate to produce maps resolving the global integral.

b. Representative integral

If correlation length scales used in the objective mapping are small compared to spatial scales of the gaps in the distribution of data, or if data are too few to overcome the noise to signal ratio used, the mapping will be inadequate in resolving the global integral. To circumvent this problem larger scales could be added to the correlation length scale, however there is no obvious physical basis for these additions, and they would lead to vastly larger matrices that would require significant computing resources to invert. An alternative option is to integrate only where there are data rather than in terms of the mapped fields, $obs_k = obs_k'' + m_{rep}$ such that, $\sum_{\substack{i=0,I \\ j=0,J}} \langle obs_k'' \rangle_{i,j} dA_{i,j} \equiv 0$, and m_{rep} is a representative spatial mean. Noting that m_{rep} is a spatial constant, (A2) can be rewritten as,

$$I_o = m_{rep} \sum_{\substack{i=0,I \\ j=0,J}} \langle 1_k \rangle_{i,j} \, dA_{i,j}, \tag{A5}$$

where $\langle 1_k \rangle_{i,j}$ is an objective map to location i, j where the data at positions k have been replaced by the value 1.

If m_t is estimated by m_{rep}, then by substituting (A5) into (A1) the true integral can be estimated by the representative integral,

$$I_t \approx \frac{I_o A}{\sum_{\substack{i=0,I \\ j=0,J}} \langle 1_k \rangle_{i,j} \, dA_{i,j}}. \tag{A6}$$

The map $\langle 1_k \rangle_{i,j}$ is a representation of the fraction of area for a given data distribution, obs_k, and

$$\frac{\sum_{\substack{i=0,I \\ j=0,J}} \langle 1_k \rangle_{i,j} \, dA_{i,j}}{A} \tag{A7}$$

is the fraction of the area that is represented in the global integral of the mapped observations, I_o (A5). The quantity

$$\frac{\sum_{\substack{i=0,I \\ j=0,J}} \langle 1_k \rangle_{i,j} \, dA_{i,j}}{A} \tag{A8}$$

also represents the fraction of ocean represented in a given map by a particular data distribution.

REFERENCES

AchutaRao, K., M. Ishii, B. D. Santer, P. J. Gleckler, K. E. Taylor, T. P. Barnett, D. W. Pierce, R. J. Stouffer, and T. M. L. Wigley, 2007: Simulated and observed variabilty in ocean temperature and heat content. *Proc. Na. Acad. of Sci.*, **104,** 10 768–10 773.

AchutaRao, K. M., B. D. Santer, P. J. Gleckler, K. E. Taylor, D. W. Pierce, T. P. Barnett, and T. M. L. Wigley, 2006: Variability of ocean heat uptake: Reconciling observations and models. *J. Geophys. Res*, **111,** 20.

Boyer, T. P., J. I. Antonov, H. Garcia, D. R. Johnson, R. A. Locarnini, A. V. Mishonov, M. T. Pitcher, O. K. Baranova, and I. Smolyar, 2006: World Ocean Database 2005, Chapter 1: Introduction, NOAA Atlas NESDIS 60, S. Levitus Ed., U.S. Government Printing Office, Washington, D.C., 182 pp., DVD.

Ducet, N., P. Y. Le Traon, and G. Reverdin, 2000: Global high-resolution mapping of ocean circulation from TOPEX/Poseidon and ERS-1 and-2. *J. Geophys. Res*, **105,** 19 477–19 498.

Gille, S. T., 2007: Decadal-Scale Temperature Trends in the Southern Hemisphere Ocean. *J. Clim.,* submitted.

Gilson, J., D. Roemmich, B. Cornuelle, and L. L. Fu, 1998: Relationship of TOPEX/Poseidon altimetric height to steric height and circulation in the North Pacific. *J. Geophys. Res.*, **103,** 27 947–27 965.

Gouretski, V. V., and P. Koltermann, 2007: How much is the ocean really warming? *Geophys. Res. Lett.*, **37,** L01610, doi:10.1029/2006GL027834.

Gregory, J. M., H. T. Banks, P. A. Stott, J. A. Lowe, and M. D. Palmer, 2004: Simulated and observed decadal variability in ocean heat content. *Geophys. Res. Lett.*, **31,** L14614, doi:10.1029/2006GL026769.

Hansen, J., L. Nazarenko, R. Ruedy, M. Sato, J. Willis, A. Del Genio, D. Koch, A. Lacis, K. Lo, S. Menon, T. Novakov, J. Perlwitz, G. Russell, G. A. Schmidt, and N. Tausnev, 2005: Earth's energy imbalance: Confirmation and implications. *Science*, **308,** 1431–1435.

Harrison, D. E. and M. Carson, 2007: Is the world ocean warming? Upper-ocean temperature trends: 1950–2000. *J. Phys. Oceanogr.*, **37,** 174–187.

Ishii, M., M. Kimoto, K. Sakamoto, and S. Iwasaki, 2006: Steric sea level changes estimated from historical ocean subsurface temperature and salinity analyses *J. Oceanogr.*, **62,** 155–170.

Levitus, S., J. Antonov, and T. Boyer, 2005: Warming of the world ocean, 1955–2003. *Geophys. Res. Lett.*, **32,** L02604, doi:10.1029/2004GL021592.

Lyman, J. M., J. K. Willis, and G. C. Johnson, 2006: Recent cooling of the upper ocean. *Geophys. Res. Lett.*, **33,** L18604, doi:10.1029/2006GL027033.

Pierce, D. W., T. P. Barnett, K. M. AchutaRao, P. J. Gleckler, J. M. Gregory, and W. M. Washington, 2006: Anthropogenic warming of the oceans: Observations and model results. *J. Clim.*, **19,** 1873–1900.

White, W. B. and C. K. Tai, 1995: Inferring interannual changes in global upper ocean heat storage from TOPEX altimetry. *J. Geophys. Res.*, **100,** 24 943–24 954.

Wijffels, S. E., J. K. Willis, C. Doingues, P. Barker, N. White, A. Gronell, K. Ridgeway, and J. Church. Changing eXpendable BathyThermograph fall rates and their impact on estimates of thermosteric sea level rise. Draft manuscript.

Willis, J., J. M. Lyman, G. C. Johnson, and J. Gilson, 2007a: Correction to "Recent cooling of the upper ocean". *Geophys. Res. Lett.*, **34, L16601** doi:10.1029/2007GL030323.

——, 2007b: In stiu data biases and recent ocean heat content variability. *Geophys. Res. Lett.*, submitted.

Willis, J. K., D. Roemmich, and B. Cornuelle, 2004: Interannual variability in upper ocean heat content, temperature, and thermosteric expansion on global scales. *J. Geophys. Res.* **109,** 13, c12036, doi: 10.1029/2003JC002260.

Wunsch, C. 1996. The Ocean Circulation Inverse Problem, Cambridge University Press, pp. 442.

Wunsch, C., R. Ponte, and P. Heimbach, 2007: Decadal trends in sea level patterns: 1993–2004. *J. Clim.* submitted.

Zang, X. Y., and C. Wunsch, 2001: Spectral description of low-frequency oceanic variability. *J. Phys. Oceanogr.*, **31,** 3073–3095.

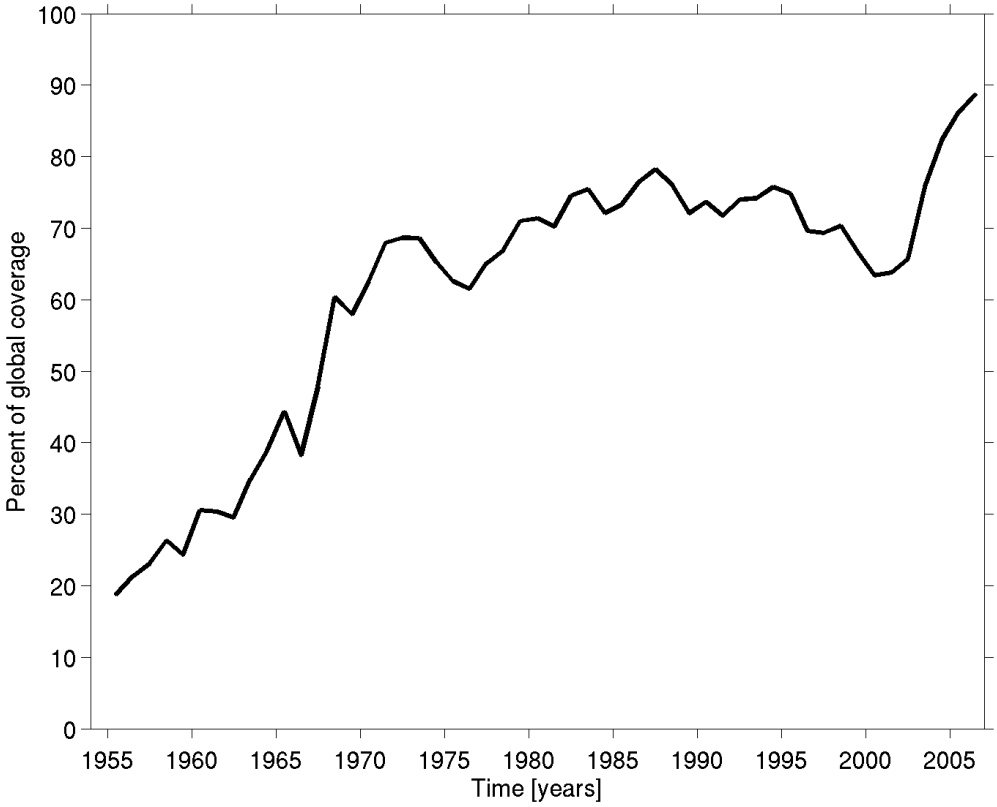

Figure 1. Percentage of global ice-free ocean sampled for in situ upper (0–750 m) Ocean Heat Content Anomaly (OHCA) for each calendar year (see Appendix A).

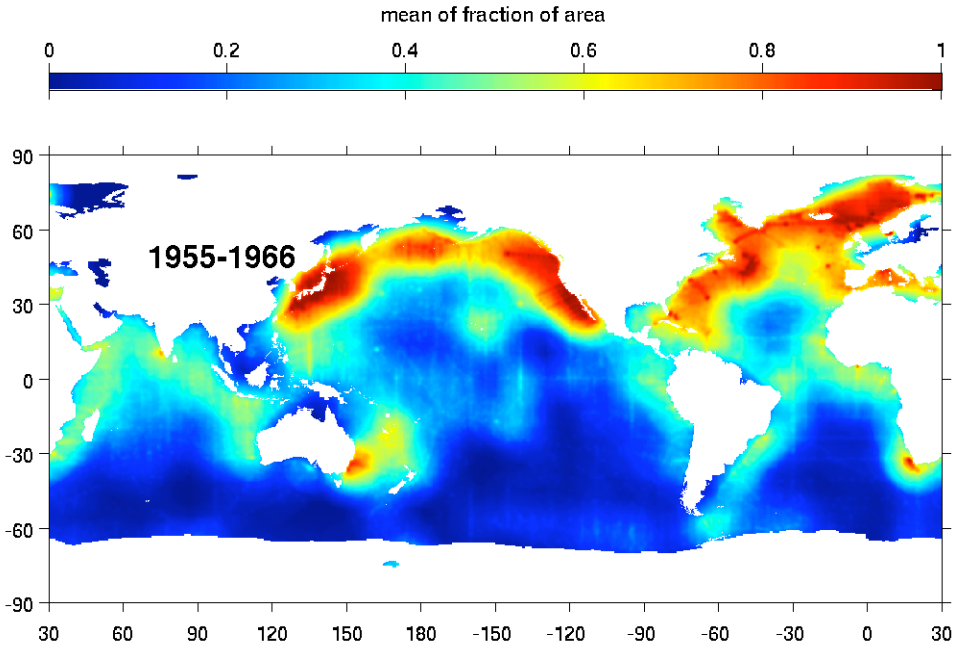

Figure 2. Mean of annual area coverage (see Appendix A) from 1955 to 1966.

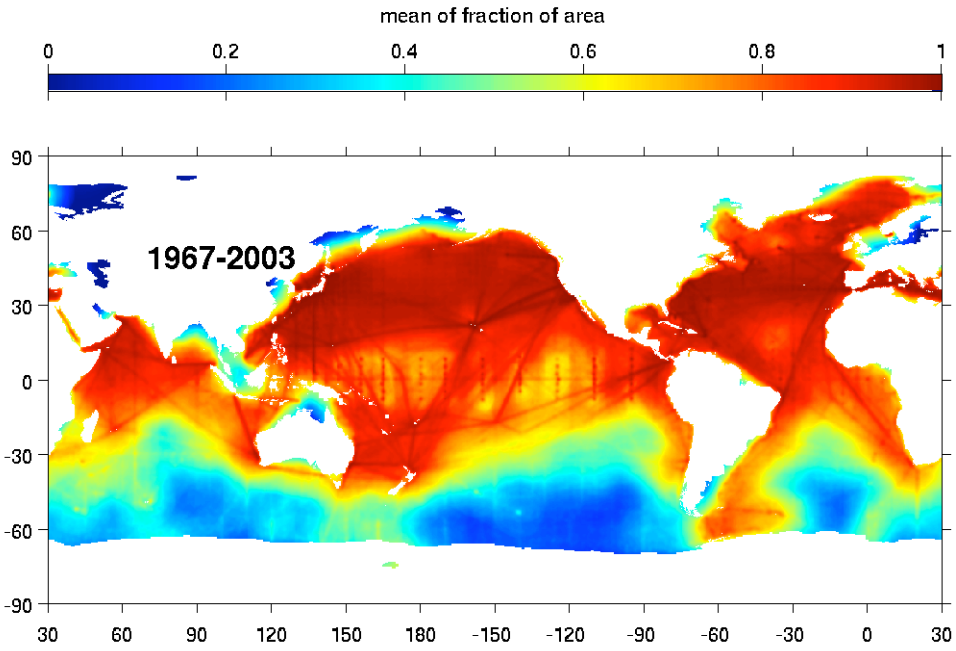

Figure 3. Mean of annual area coverages from 1967 to 2003.

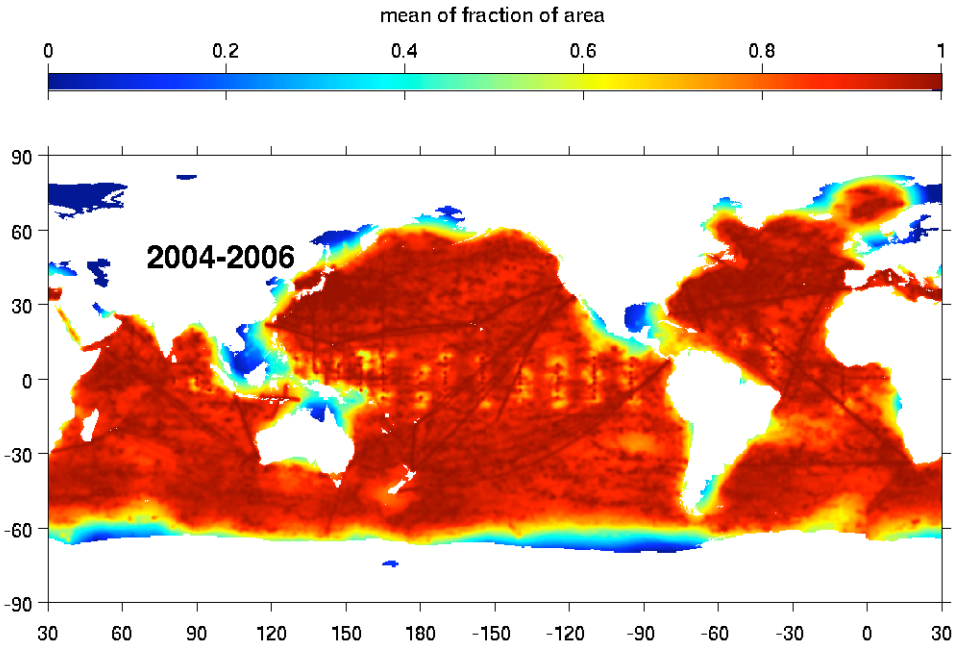

Figure 4. Mean of annual area coverages from 2004 to 2006.

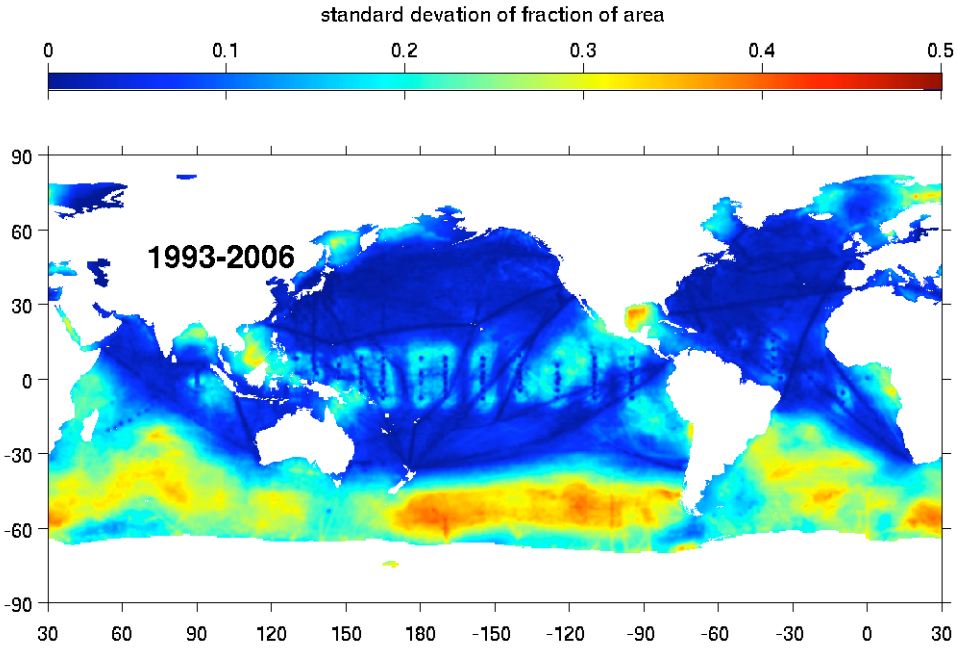

Figure 5. Standard devation of annual area coverages from 1993–2006 based on 14 one-year maps.

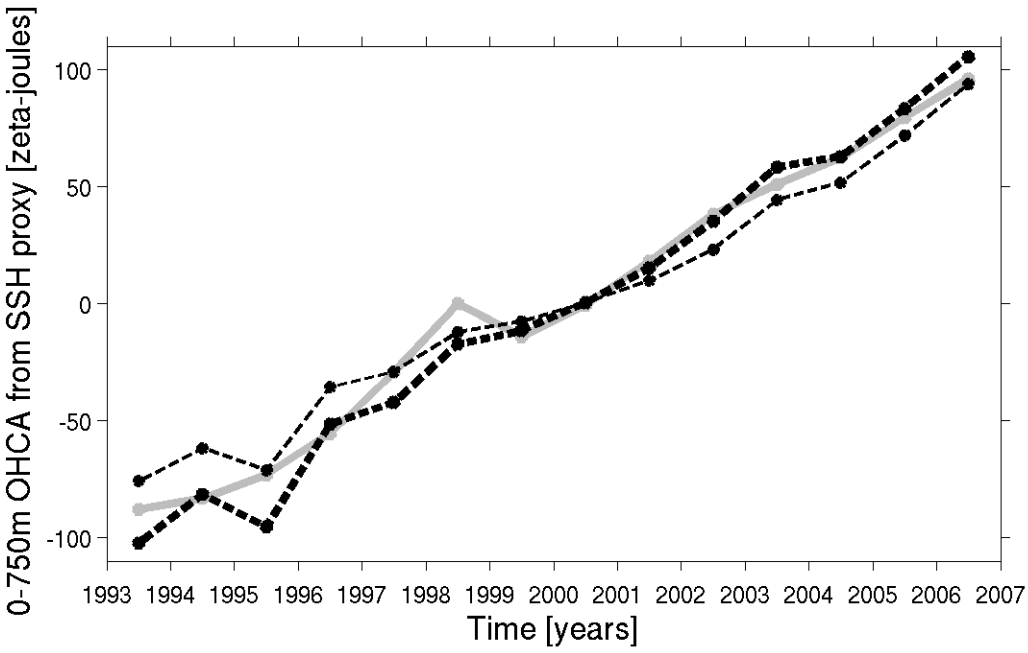

Figure 6. Annual global integrals of synthetic OHCA in the upper 750 m estimated from Aviso SSH. When computed from the entire Aviso record (thick gray line) the OCHA curve has a linear trend of 0.9 ± 0.1 W m^{-2}, a linear trend of 0.8 ± 0.1 W m^{-2} when computed from the integrals of subsampled synthetic OHCA (thin dashed line), and a linear trend of 1.0 ± 0.1 W m^{-2} when computed from representative integrals of subsampled synthetic OHCA (thick dashed line).

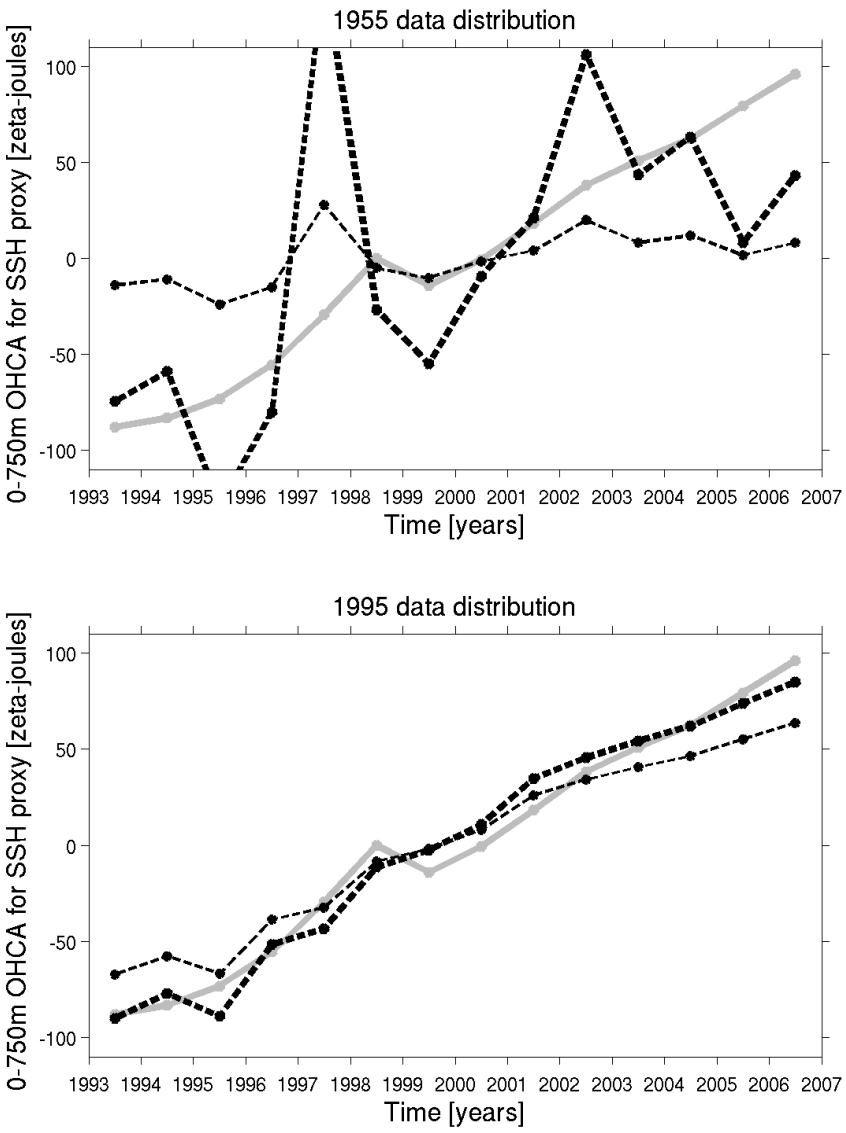

Figure 7. Following Fig. 6, but for global OHCA integrals from the Aviso SSH record subsampled at 1955 (upper panel) and 1995 (lower panel) in situ data locations. For the 1955 data distribution the trend computed from integrals of the maps is 0.1 ± 0.1 W m^{-2} and 0.7 ± 0.7 W m^{-2} from representative integrals. For the 1995 data distribution the trend from integrals of the maps is 0.7 ± 0.1 W m^{-2} and 0.9 ± 0.1 W m^{-2} from representative integrals.

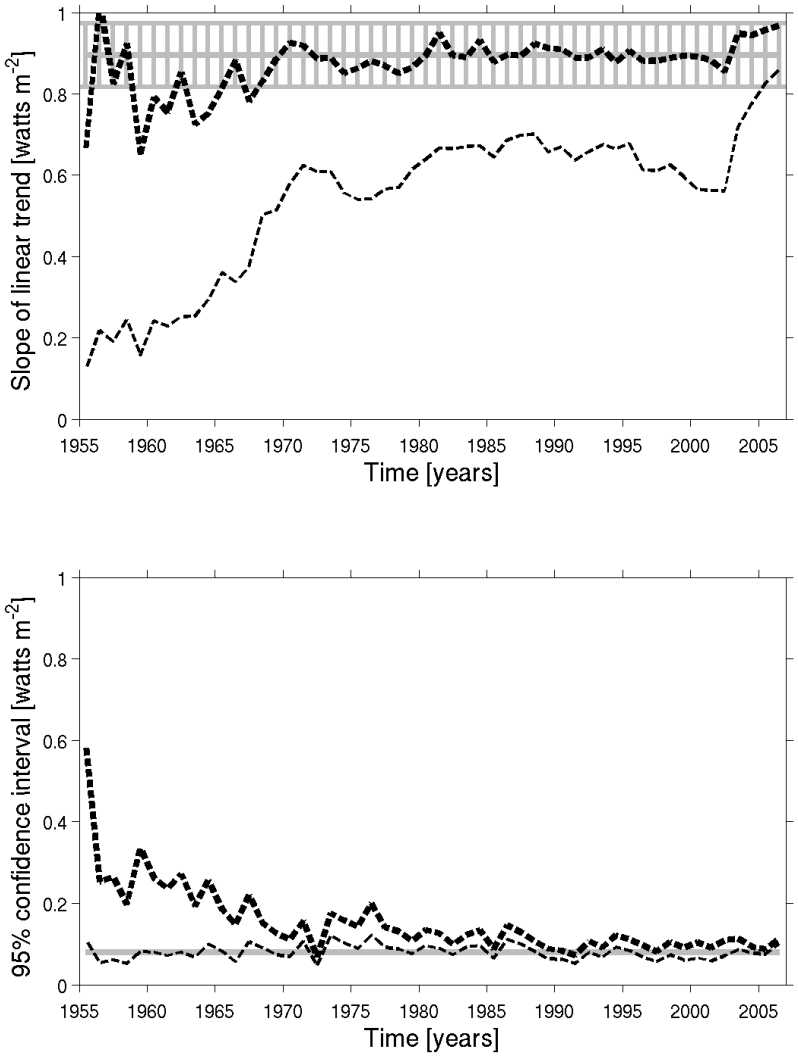

Figure 8. Summary of 13-year warming trends (upper panel) and their 95% confidence intervals (lower panel) plotted as a function of each year's data distrbution from 1955 through 2006 for the entire synthetic estimates of OHCA (grey lines), the synthetic estimates computed from integrals of the maps (thin dashed lines), and the synthetic estimates computed from representative integrals (thick dashed lines). Only the confidence intervals for the entire synthetic estimate (lower panel) are shown in the upper panel.

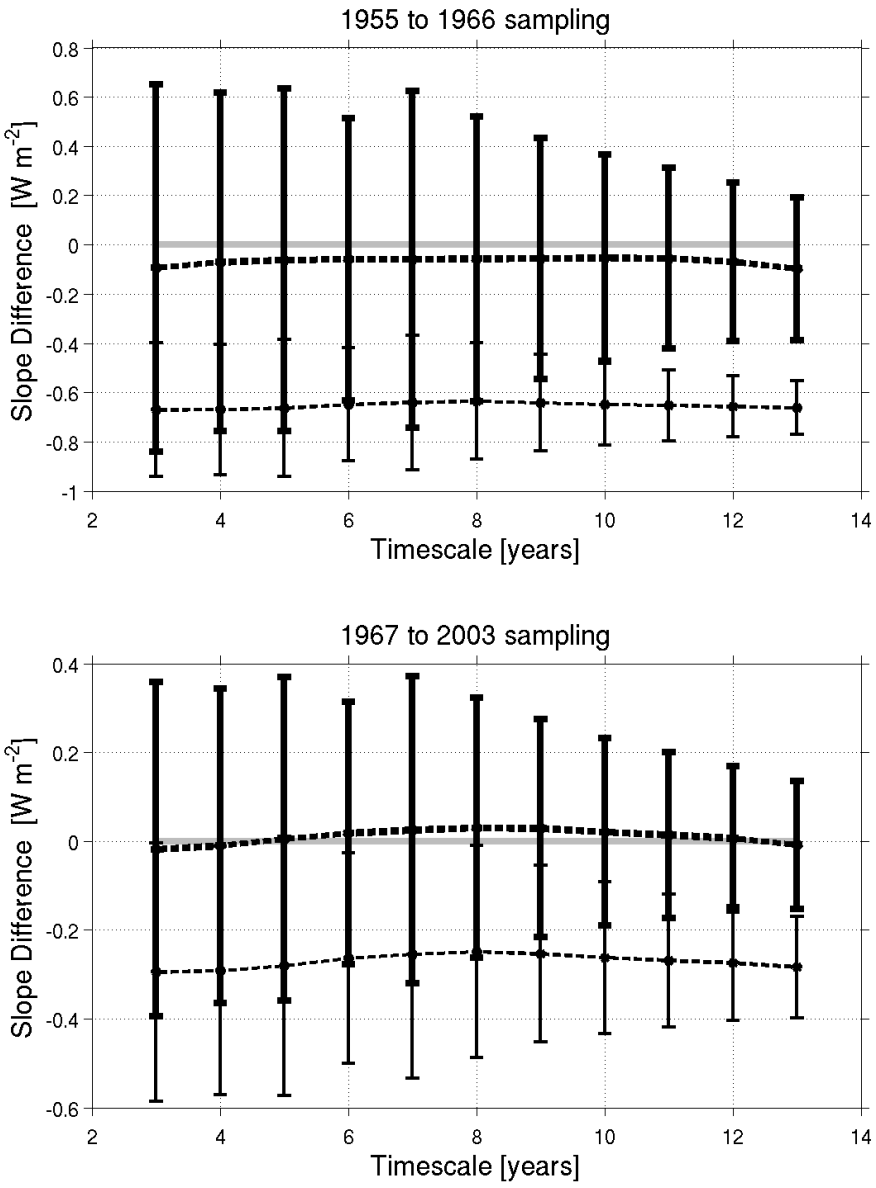

Figure 9. Mean differences in the true linear trend and the trend computed from both integrals of the maps (thin dashed line) and representative integrals (thick dashed line) for 3- to 13-year time scales. Differences are averaged over all possible segments of the time series for sampling patterns from 1955 to 1966 (upper panel) and 1967 to 2003 (lower panel). Error bars are 95% confidence intervals.

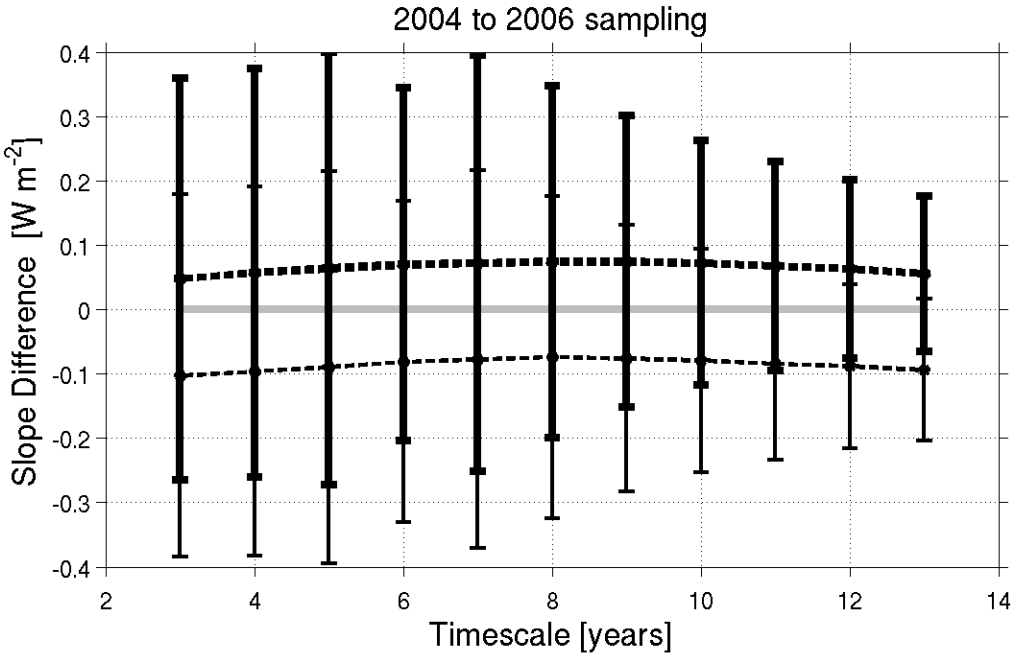

Figure 10. Following Fig. 9 but for sampling patterns from 2004 to 2006.

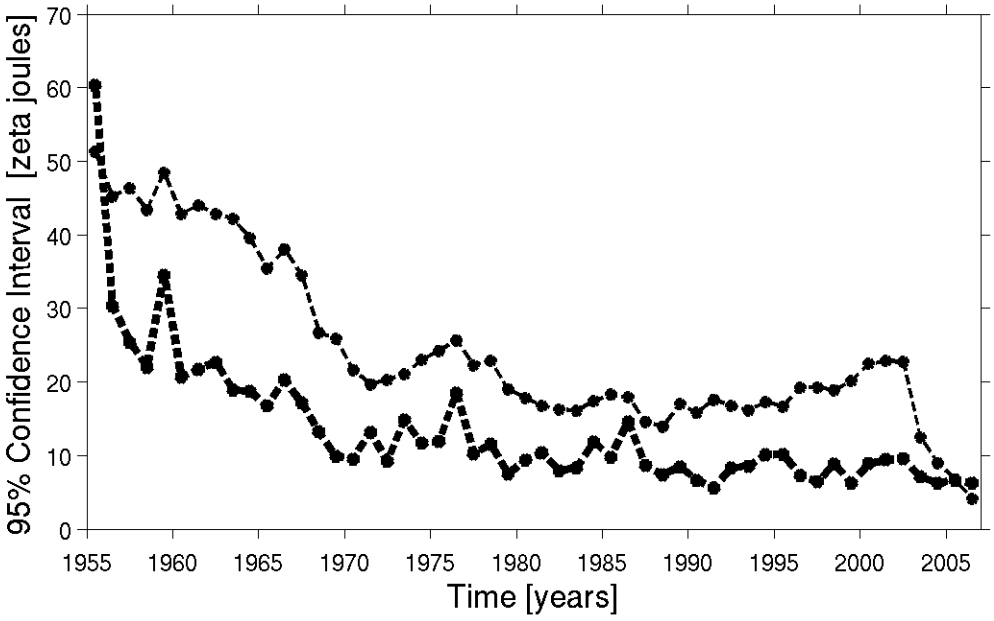

Figure 11. Sampling error computed following Lyman et al. (2006) from synthetic estimates of globally integrated OHCA both for integrals of the maps (thin dashed line) and representative integrals (thick dashed line) for each year's data distribution.